Gravitational waves from the sound of a first order phase transition

Mark Hindmarsh,[1,2,*] Stephan J. Huber,[1,†] Kari Rummukainen,[2,‡] and David J. Weir[2,§]

[1] *Department of Physics and Astronomy, University of Sussex, Falmer, Brighton BN1 9QH, U.K.*
[2] *Department of Physics and Helsinki Institute of Physics, PL 64, FI-00014 University of Helsinki, Finland*

(Dated: January 30, 2014)

We report on the first 3-dimensional numerical simulations of first-order phase transitions in the early universe to include the cosmic fluid as well as the scalar field order parameter. We calculate the gravitational wave (GW) spectrum resulting from the nucleation, expansion and collision of bubbles of the low-temperature phase, for phase transition strengths and bubble wall velocities covering many cases of interest. We find that the compression waves in the fluid continue to be a source of GWs long after the bubbles have merged, a new effect not taken properly into account in previous modelling of the GW source. For a wide range of models the main source of the GWs produced by a phase transition is therefore the sound the bubbles make.

PACS numbers: 64.60.Q-, 47.75.+f, 95.30.Lz

arXiv:1304.2433v2 [hep-ph] 29 Jan 2014

In a hot Big Bang there were phase transitions in the early Universe [1, 2], which may well have been of first order; one major consequence of such a transition would be the generation of gravitational waves [3–8]. The electroweak transition in the Standard Model is known to be a cross-over [9–11] but it may be first order in minimal extensions of the Standard Model [12–17]. It is therefore essential to properly characterise the expected power spectrum from first-order phase transitions.

First order phase transitions proceed by the nucleation, growth, and merger of bubbles of the low temperature phase [3, 18–25]. The collision of the bubbles is a violent process, and both the scalar order parameter and the fluid of light particles generate gravitational waves.

Numerical studies have been carried out of the behaviour of bubbles in such a phase transition using spherically symmetric $(1+1)$-dimensional simulations [23, 24]. The calculation of the gravitational wave spectrum has been refined in the intervening years, notably using the semi-analytic envelope approximation [5, 7, 8, 26, 27] (but see Ref. [28] for an alternative approach). Fully three-dimensional simulations of the scalar field only have been carried out [29], qualitatively supporting the envelope approximation, and pointing out important gravitational wave production from the scalar field after the bubble merger.

In a hot phase transition, the fluid plays an important role, firstly as a brake on the scalar field, and secondly as a source of gravitational waves itself. The fluid has generally been assumed to be incompressible and turbulent [30–33]. An important question for the gravitational wave power spectrum is the validity of this modelling, which generally borrows from the Kolmogorov theory of non-relativistic driven incompressible turbulence.

In this Letter we report on the first fully three dimensional simulation of bubble nucleation involving a coupled field-fluid system. We make use of these simulations to calculate the power spectrum of gravitational radiation from a first-order phase transition, for a range of transition strengths and bubble wall velocities relevant for an electroweak transition in extensions of the Standard Model. We find that the compression waves in the fluid – sound waves – continue to be an important source of gravitational waves for up to a Hubble time after the bubble merger has completed. This boosts the signal by the ratio of the Hubble time to the transition time, which can be orders of magnitude.

The system describing the matter in the early universe consists of a relativistic fluid coupled to a scalar field, which acquires an effective potential

$$V(\phi,T)=\frac{1}{2}\gamma(T^2-T_0^2)\phi^2-\frac{1}{3}\alpha T\phi^3+\frac{1}{4}\lambda\phi^4. \qquad (1)$$

The rest-frame pressure p and energy density ϵ are

$$\epsilon=3aT^4+V(\phi,T)-T\frac{\partial V}{\partial T},\quad p=aT^4-V(\phi,T) \qquad (2)$$

with $a=(\pi^2/90)g$, and g the effective number of relativistic degrees of freedom contributing to the pressure at temperature T. The stress-energy tensor for a scalar field ϕ and an ideal relativistic fluid U^μ is

$$T^{\mu\nu}=\partial^\mu\phi\partial^\nu\phi-\tfrac{1}{2}g^{\mu\nu}(\partial\phi)^2+[\epsilon+p]\,U^\mu U^\nu+g^{\mu\nu}p \qquad (3)$$

where the metric convention is $(-\,+\,+\,+)$. The scalar field potential is included in the definition of p. We split $\partial_\mu T^{\mu\nu}=0$ (nonuniquely) into field and fluid parts with a dissipative term permitting transfer of energy between the scalar field and the fluid $\delta^\nu=\eta U^\mu\partial_\mu\phi\partial^\nu\phi$ [22, 23]. This simplified model can be improved, but is adequate for parametrising the entropy production [24].

Given these expressions, the equations of motion can be derived. For the field we have

$$-\ddot{\phi}+\nabla^2\phi-\frac{\partial V}{\partial\phi}=\eta W(\dot{\phi}+V^i\partial_i\phi) \qquad (4)$$

where W is the relativistic γ-factor and V^i is the fluid 3-velocity, $U^i=WV^i$. For the fluid energy density $E=$

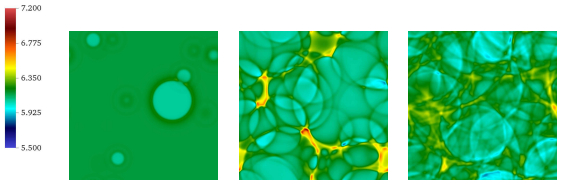


FIG. 1: Slices of fluid energy density E/T_c^4 at $t = 400\,T_c^{-1}$, $t = 800\,T_c^{-1}$ and $t = 1200\,T_c^{-1}$ respectively, for the $\eta = 0.2$ simulation. The slices correspond roughly to the end of the nucleation phase, the end of the initial coalescence phase and the end of the simulation.

$W\epsilon$, contracting $[\partial_\mu T^{\mu\nu}]_{\rm fluid}$ with U_ν yields

$$\dot{E} + \partial_i(EV^i) + p[\dot{W} + \partial_i(WV^i)] - \frac{\partial V}{\partial\phi}W(\dot{\phi} + V^i\partial_i\phi) = \eta W^2(\dot{\phi} + V^i\partial_i\phi)^2. \quad (5)$$

The equations of motion for the fluid momentum density $Z_i = W(\epsilon + p)U_i$ read

$$\dot{Z}_i + \partial_j(Z_iV^j) + \partial_i p + \frac{\partial V}{\partial\phi}\partial_i\phi = -\eta W(\dot{\phi} + V^j\partial_j\phi)\partial_i\phi. \quad (6)$$

The principal observable of interest to us is the power spectrum of gravitational radiation resulting from bubble collisions. One approach is to project T_{ij} at every timestep and then making use of the Green's function to compute the final power spectrum [34, 35]; this is quite costly in computer time. Instead, we use the procedure detailed in Ref. [36]. We evolve the equation of motion for an auxiliary tensor u_{ij},

$$\ddot{u}_{ij} - \nabla^2 u_{ij} = 16\pi G(\tau^\phi_{ij} + \tau^{\rm f}_{ij}), \quad (7)$$

where $\tau^\phi_{ij} = \partial_i\phi\partial_j\phi$ and $\tau^{\rm f}_{ij} = W^2(\epsilon + p)V_iV_j$. The physical metric perturbations are recovered in momentum space by $h_{ij}(\mathbf{k}) = \lambda_{ij,lm}(\hat{\mathbf{k}})u_{lm}(t,\mathbf{k})$, where $\lambda_{ij,lm}(\hat{\mathbf{k}})$ is the projector onto transverse, traceless symmetric rank 2 tensors. We are most interested in the metric perturbations sourced by the fluid, as the fluid shear stresses generally dominate over those of the scalar field, although it will be instructive to also consider both sources together.

Having obtained the metric perturbations, the power spectrum per logarithmic frequency interval is

$$\frac{d\rho_{\rm GW}(k)}{d\ln k} = \frac{1}{32\pi GL^3}\frac{k^3}{(2\pi)^3}\int d\Omega\,\left|\dot{h}_{lm}(t,\mathbf{k})\right|^2. \quad (8)$$

We simulate the system on a cubic lattice of $N^3 = 1024^3$ points, neglecting cosmic expansion which is slow compared with the transition rate. The fluid is implemented as a three dimensional relativistic fluid [37], with donor cell advection. The scalar and tensor fields are evolved using a leapfrog algorithm with a minimal stencil for the spatial Laplacian. Principally we used lattice spacing $\delta x = 1\,T_c^{-1}$ and time step $\delta t = 0.1\,T_c^{-1}$, where T_c is the critical temperature for the phase transition. We have checked the lattice spacing dependence by carrying out single bubble self-collision simulations for $L^3 = 256^3\,T_c^{-3}$ at $\delta x = 0.5\,T_c^{-1}$, for which the value of $\rho_{\rm GW}$ at $t = 2000T_c^{-1}$ increased by 10%, while the final total fluid kinetic energy increased by 7%. Simulating with $\delta t = 0.2\,T_c^{-1}$ resulted in changes of 0.3% and 0.2% to $\rho_{\rm GW}$ and the kinetic energy respectively.

Starting from a system completely in the symmetric phase, we model the phase transition by nucleating new bubbles according to the rate per unit volume $P = P_0\exp(\beta(t - t_0))$. From this distribution we generate a set of nucleation times and locations (in a suitable untouched region of the box) at each of which we insert a static bubble with a gaussian profile for the scalar field. The bubble expands and quickly approaches an invariant scaling profile [23].

We first studied a system with $g = 34.25$, $\gamma = 1/18$, $\alpha = \sqrt{10}/72$, $T_0 = T_c/\sqrt{2}$ and $\lambda = 10/648$; this allows comparison with previous $(1+1)$ and spherical studies of a coupled field-fluid system where the same parameter choices were used [23]. The transition in this case is relatively weak: in terms of α_T, the ratio between the latent heat and the total thermal energy, we have $\alpha_{T_N} = 0.012$ at the nucleation temperature $T_{\rm N} = 0.86\,T_c$. We also performed simulations with $\gamma = 2/18$ and $\lambda = 5/648$, for which $\alpha_{T_N} = 0.10$ at the nucleation temperature $T_{\rm N} = 0.8\,T_c$, which we refer to as an intermediate strength transition. We note that $\alpha_{T_N} \sim 10^{-2}$ is generic for a first order electroweak transition, while $\alpha_{T_N} \sim 10^{-1}$ would imply some tuning [38].

For the nucleation process, we took $\beta = 0.0125\,T_c$, $P_0 = 0.01$ and $t_0 = t_{\rm end} = 2000\,T_c^{-1}$. The simulation volume allowed the nucleation of 100-300 bubbles, so that the mean spacing between bubbles was of order $100\,T_c^{-1}$. The wall velocity is captured correctly, but the fluid velocity did not quite reach the scaling profile before colliding. Typically, the peak velocity prior to collision is 20-30% below the scaling value for the deflagrations.

For the weak transition we chose $\eta = 0.1$, 0.2, 0.4 and 0.6. The first gives a detonation with wall speed $v_{\rm w} \simeq 0.71$, and the others weak deflagrations with $v_{\rm w} \simeq 0.44$, 0.24, and 0.15 respectively. The shock profiles are found in Figs. 2 and 3 of Ref. [23]; slices of the total energy density for one of our simulations are shown in Fig. 1. The intermediate transition was simulated at $\eta = 0.4$, for which the wall speed is $v_{\rm w} \simeq 0.44$, very close to the weak transition with $\eta = 0.2$.

Fig. 2 (top) shows the time evolution of two quantities

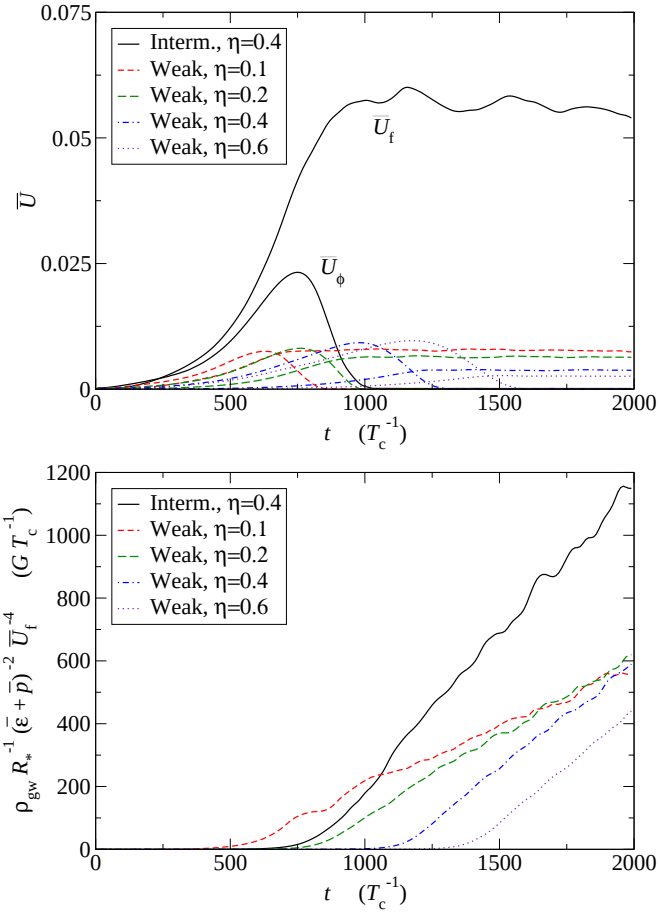


FIG. 2: Top: time series of $\overline{U}_\phi$ and $\overline{U}_\mathrm{f}$ (9), showing the progress of the phase transition; the curves for $\overline{U}_\phi$ and $\overline{U}_\mathrm{f}$ are individually identified for the 'intermediate' case. Bottom: time series of $\rho_\mathrm{GW} R_*^{-1}[(\bar{\epsilon}+\bar{p})^{-2}\overline{U}_\mathrm{f}^{-4}]_{t_\mathrm{end}}$, showing the evolution of the gravitational wave energy density relative to an estimate of the square of the final fluid shear stresses.

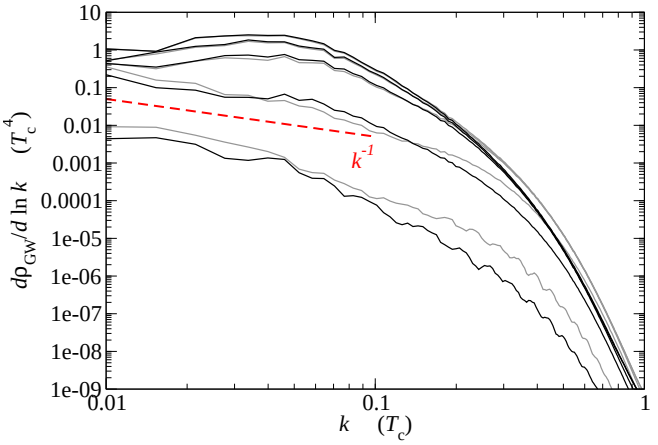


FIG. 3: Gravitational wave power spectra during the phase transition, for the intermediate strength transition, from fluid only (black) and both fluid and field (grey). From bottom to top, the times are $t = 600$, 800, 1000, 1200 and $1400\,T_\mathrm{c}^{-1}$. The red dashed line indicates the expected k^{-1} behaviour.

$\overline{U}_\phi$ and $\overline{U}_\mathrm{f}$, defined so that

$$(\bar{\epsilon}+\bar{p})\overline{U}_\phi^2 = \frac{1}{V}\int d^3x \tau_{ii}^\phi \quad \text{and} \quad (\bar{\epsilon}+\bar{p})\overline{U}_\mathrm{f}^2 = \frac{1}{V}\int d^3x \tau_{ii}^\mathrm{f} \tag{9}$$

where $\bar{\epsilon}$ and $\bar{p}$ are the time-dependent, volume-averaged rest-frame energy density and pressure respectively.

The squares of these quantities give an estimate of the size of the shear stresses of the field and the fluid relative to the background fluid enthalpy density, while $\overline{U}_\mathrm{f}$ tends to the r.m.s. fluid velocity for $\overline{U}_\mathrm{f} \ll 1$. We see that $\overline{U}_\phi$ grows and decays with the total surface area of the bubbles of the new phase, while the mean fluid velocity grows with the volume of the bubbles, and then stays constant once the bubbles have merged. We have no explicit viscosity, and the slight decreasing trend in $\overline{U}_\mathrm{f}$, visible for the intermediate transition, arises from the well-known numerical viscosity of donor-cell advection, $\nu_\mathrm{num} \simeq \overline{U}_\mathrm{f}\delta x$.

Fig. 2 (bottom) shows the GW energy density scaled by the final value of $(\bar{\epsilon}+\bar{p})^2\overline{U}_\mathrm{f}^4$ and the average bubble size at collision $R_* = L/N_\mathrm{b}^{1/3}$, where N_b is the number of bubbles in the simulation volume. The scaling enables comparison to a model discussed around Eq. (12), which predicts a linear growth in ρ_GW at late times, sourced by persistent perturbations in the fluid. The GW energy density rises linearly after the bubbles have fully merged with similar slopes, which supports the model. Note that the GWs from detonations ($\eta = 0.1$) behave similarly to those from deflagrations.

In Fig. 3 we show the time development of the GW power spectrum as the intermediate strength phase transition proceeds. We see that strong growth happens between $t = 600\,T_\mathrm{c}^{-1}$ and $t = 1000\,T_\mathrm{c}^{-1}$ as the bubbles merge (see Fig. 2). For $t \lesssim 1000\,T_\mathrm{c}^{-1}$ there is evidence of the expected k^{-1} power spectrum, but it becomes less clear as the GW power continues to grow, sourced by the persistent fluid perturbations. At the shortest length scales, we see a v_w-dependent exponential fall-off.

To establish the nature of these fluid perturbations, we show in Fig. 4 the time development of the longitudinal (compressional) and transverse (rotational) components of the fluid velocity power spectrum. At all times, it is clear that most of the fluid velocity is longitudinal, indicating that the perturbations are mostly compression waves. Turbulence generally develops at high Reynolds number Re in the transverse components, characterised by a power-law behaviour of the power spectrum. Given the bubble separation scale R_*, we can estimate the value of Re, due entirely to the numerical viscosity, as $\mathrm{Re}_\mathrm{num} = \overline{U}_\mathrm{f} R_*/\nu_\mathrm{num} \sim 10^2$. There is no firm evidence of a power law at high k, but it is unclear whether Re is large enough for turbulence to develop here.

We can now form a clearer picture of the fluid per-

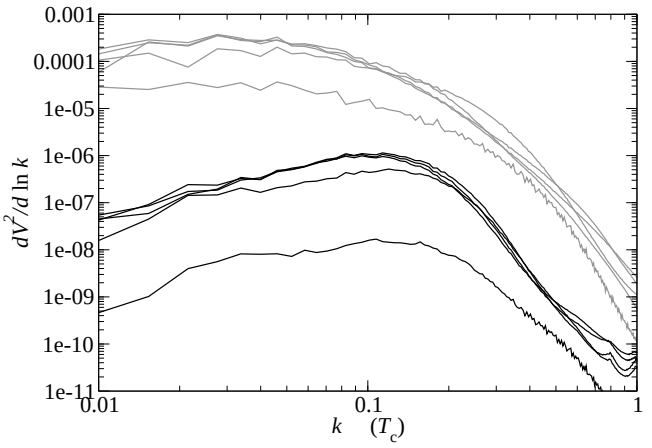


FIG. 4: Fluid velocity power spectra for the intermediate strength transition, separated into longitudinal (compressional) and transverse (rotational) components; shown in grey and black respectively. Times shown are the same as Fig. 3.

turbations and how the GWs are generated. Firstly, we note that the fluid perturbations are initially the form of a compression wave surrounding the growing bubble. The energy in this wave is proportional to the volume of the bubble R^3, and quickly outstrips the energy in the scalar field, which grows only as R^2. The energy in the compression waves remains constant after the bubbles have merged. This is due to linearity and conservation of energy: as the fluid velocities are generally small, there is little transfer to the transverse components.

The bubble collision generates gravitational waves, as predicted by the envelope approximation, and there is some evidence for the characteristic k^{-1} spectrum between R_* and the high-frequency cut-off. The generation of GWs continues long after the merger is completed and the scalar field has relaxed to its new equilibrium value. The GWs are sourced by the compression waves in the fluid. This source of gravitational radiation from a phase transition – sound – has not been appreciated before (except in Ref. [4]).

The resulting density of the gravitational waves is given from the unequal time correlator of the shear stress tensor $\Pi^2(k,t_1,t_2)$ by [27, 39]

$$\frac{d\rho_{\rm GW}(k)}{d\ln k} = \frac{2Gk^3}{\pi}\int^t dt_1 dt_2 \cos[k(t_1-t_2)]\Pi^2(k,t_1,t_2). \tag{10}$$

We model the source as turning on at the nucleation time $t_{\rm N}$ with a lifetime $\tau_{\rm s}$ (discussed below), and being a function of t_1-t_2 between those times, as is reasonable for stochastic sound waves. We suppose the correlator is peaked at $t_1-t_2=0$ with width $x_{\rm c}/k$, where $x_{\rm c}$ is a dimensionless parameter. This resembles the "top-hat" correlator model of Ref. [27], except that the source acts for much longer than the duration of the transition β^{-1}. We estimate the amplitude of the source as $\left[(\bar\epsilon+\bar p)\overline{U}_{\rm f}^2\right]^2$, and its length scale as R_*. Hence, for $t_{\rm N}<(t_1,t_2)<\tau_{\rm s}$,

$$\Pi^2(k,t_1,t_2) \simeq [(\bar\epsilon+\bar p)\overline{U}_{\rm f}^2]^2 R_*^3 \tilde\Pi^2(kR_*, z/x_{\rm c}), \tag{11}$$

where $z=k(t_1-t_2)$ and $\tilde\Pi^2$ is dimensionless. The density parameter $\Omega_{\rm GW}=\rho_{\rm GW}/\bar\epsilon$ is then

$$\Omega_{\rm GW} \simeq \frac{3\bar\Pi^2}{4\pi^2}(H_*\tau_{\rm s})(H_*R_*)(1+w)^2\overline{U}_{\rm f}^4, \tag{12}$$

where H_* is the Hubble parameter at the transition, $w=\bar p/\bar\epsilon\simeq 1/3$, and

$$\bar\Pi^2 = \int d\ln k\,(kR_*)^2 \int dz\cos(z)\tilde\Pi^2(kR_*,z/x_{\rm c}). \tag{13}$$

In Eq. (12) we see the origin of the R_* factor in the GW density, which must be present for dimensional reasons. The slope of the curves in Fig. (2, bottom) is $2\bar\Pi^2/\pi$, which we see takes the natural value O(1), and is weakly dependent on the transition parameters.

The envelope approximation gives [26]

$$\Omega_{\rm GW} \simeq \frac{0.11 v_{\rm w}^3}{0.42+v_{\rm w}^2}\left(\frac{H_*}{\beta}\right)^2 \frac{\kappa^2\alpha_T^2}{(\alpha_T+1)^2} \tag{14}$$

where κ is the efficiency with which latent heat is converted to kinetic energy. Comparing to (12) and noting that $\overline{U}_{\rm f}^4\sim\kappa^2\alpha_T^2$, $R_*\sim v_{\rm w}/\beta$, we see that sound waves are parametrically larger by the factor $\tau_{\rm s}/R_*v_{\rm w}$.

An upper bound on $\tau_{\rm s}$ is the Hubble time, as the shear stresses decay faster than the background energy density. The shear stresses also decay due to the viscosity $\eta_{\rm s}$, which can be estimated as $\eta_{\rm s}\sim T^3/e^4\ln(1/e)$, where e is the electromagnetic gauge coupling [40]. The viscous damping time of sound waves with characteristic wavelength R_* is therefore $\tau_\eta\simeq R_*^2\bar\epsilon/\eta_{\rm s}\sim e^4\ln(1/e)R_*^2T_{\rm c}$. Hence sound waves from smaller bubbles are damped by viscosity, but live long enough to be the most important source of gravitational waves for bubbles provided

$$R_*H_* \gg v_{\rm w}(\sqrt{a}T_{\rm c}/m_{\rm P}e^4) \sim 10^{-11}v_{\rm w}(T_{\rm c}/100\ {\rm GeV}). \tag{15}$$

This is generally satisfied except for weak transitions at very high temperatures, and we conclude that for most transitions the fluid damping time is the Hubble time.

We point out that we have studied systems with non-relativistic and linear fluid velocities, without explicit viscosity. These choices are representative of a typical first order electroweak phase transition, but it would also be interesting to study strong transitions with relativistic fluid velocities, explore the effect of dissipation, and look for turbulent regimes. Parameter choices recently identified as having unstable bubble walls [41] also merit investigation. We have not studied the case where the walls run away, although here we expect that the fluid is unimportant and the envelope approximation applies.

In the cases that we do study, we find the velocity perturbations are principally acoustic waves, and that the resulting gravitational radiation density is parametrically larger than given in the envelope approximation by the ratio of the fluid damping time $\tau_{\rm s}$ to the duration of the phase transition β^{-1}. We conclude that, for a wide range of first order phase transitions of interest, the main source of the gravitational wave background is the sound they make.

Our simulations made use of facilities at the Finnish Centre for Scientific Computing CSC, and the COSMOS Consortium supercomputer (within the DiRAC Facility jointly funded by STFC and the Large Facilities Capital Fund of BIS). KR acknowledges support from the Academy of Finland project 1134018; MH and SH from the Science and Technology Facilities Council (grant number ST/J000477/1).

* Electronic address: m.b.hindmarsh@sussex.ac.uk
† Electronic address: s.huber@sussex.ac.uk
‡ Electronic address: kari.rummukainen@helsinki.fi
§ Electronic address: david.weir@helsinki.fi

[1] D. Kirzhnits, JETP Lett. **15**, 529 (1972).
[2] D. Kirzhnits and A. D. Linde, Annals Phys. **101**, 195 (1976).
[3] E. Witten, Phys.Rev. **D30**, 272 (1984).
[4] C. J. Hogan, MNRAS **218**, 629 (1986).
[5] A. Kosowsky, M. S. Turner, and R. Watkins, Phys.Rev. **D45**, 4514 (1992).
[6] A. Kosowsky, M. S. Turner, and R. Watkins, Phys.Rev.Lett. **69**, 2026 (1992).
[7] A. Kosowsky and M. S. Turner, Phys.Rev. **D47**, 4372 (1993), astro-ph/9211004.
[8] M. Kamionkowski, A. Kosowsky, and M. S. Turner, Phys.Rev. **D49**, 2837 (1994), astro-ph/9310044.
[9] K. Kajantie, M. Laine, K. Rummukainen, and M. E. Shaposhnikov, Phys.Rev.Lett. **77**, 2887 (1996), hep-ph/9605288.
[10] M. Laine and K. Rummukainen, Phys.Rev.Lett. **80**, 5259 (1998), hep-ph/9804255.
[11] M. Laine, G. Nardini, and K. Rummukainen, JCAP **1301**, 011 (2013), 1211.7344.
[12] M. S. Carena, M. Quiros, and C. Wagner, Phys.Lett. **B380**, 81 (1996), hep-ph/9603420.
[13] D. Delepine, J. Gerard, R. Gonzalez Felipe, and J. Weyers, Phys.Lett. **B386**, 183 (1996), hep-ph/9604440.
[14] M. Laine and K. Rummukainen, Nucl.Phys. **B535**, 423 (1998), hep-lat/9804019.
[15] C. Grojean, G. Servant, and J. D. Wells, Phys.Rev. **D71**, 036001 (2005), hep-ph/0407019.
[16] S. J. Huber and M. Schmidt, Nucl.Phys. **B606**, 183 (2001), hep-ph/0003122.
[17] S. J. Huber, T. Konstandin, T. Prokopec, and M. G. Schmidt, Nucl.Phys. **B757**, 172 (2006), hep-ph/0606298.
[18] P. J. Steinhardt, Phys.Rev. **D25**, 2074 (1982).
[19] H. Kurki-Suonio, Nucl.Phys. **B255**, 231 (1985).
[20] K. Kajantie and H. Kurki-Suonio, Phys.Rev. **D34**, 1719 (1986).
[21] K. Enqvist, J. Ignatius, K. Kajantie, and K. Rummukainen, Phys.Rev. **D45**, 3415 (1992).
[22] J. Ignatius, K. Kajantie, H. Kurki-Suonio, and M. Laine, Phys.Rev. **D49**, 3854 (1994), astro-ph/9309059.
[23] H. Kurki-Suonio and M. Laine, Phys.Rev. **D54**, 7163 (1996), hep-ph/9512202.
[24] H. Kurki-Suonio and M. Laine, Phys.Rev.Lett. **77**, 3951 (1996), hep-ph/9607382.
[25] J. R. Espinosa, T. Konstandin, J. M. No, and G. Servant, JCAP **1006**, 028 (2010), 1004.4187.
[26] S. J. Huber and T. Konstandin, JCAP **0809**, 022 (2008), 0806.1828.
[27] C. Caprini, R. Durrer, T. Konstandin, and G. Servant, Phys.Rev. **D79**, 083519 (2009), 0901.1661.
[28] C. Caprini, R. Durrer, and G. Servant, Phys.Rev. **D77**, 124015 (2008), 0711.2593.
[29] H. L. Child and J. Giblin, John T., JCAP **1210**, 001 (2012), 1207.6408.
[30] A. Kosowsky, A. Mack, and T. Kahniashvili, Phys.Rev. **D66**, 024030 (2002), astro-ph/0111483.
[31] G. Gogoberidze, T. Kahniashvili, and A. Kosowsky, Phys.Rev. **D76**, 083002 (2007), 0705.1733.
[32] C. Caprini and R. Durrer, Phys.Rev. **D74**, 063521 (2006), astro-ph/0603476.
[33] C. Caprini, R. Durrer, and G. Servant, JCAP **0912**, 024 (2009), 0909.0622.
[34] S. Khlebnikov and I. Tkachev, Phys.Rev. **D56**, 653 (1997), hep-ph/9701423.
[35] R. Easther and E. A. Lim, JCAP **0604**, 010 (2006), astro-ph/0601617.
[36] J. Garcia-Bellido, D. G. Figueroa, and A. Sastre, Phys.Rev. **D77**, 043517 (2008), 0707.0839.
[37] J. Wilson and G. Matthews, Relativistic Numerical Hydrodyamics (Cambridge University Press, Cambridge, 2003).
[38] S. J. Huber and T. Konstandin, JCAP **0805**, 017 (2008), 0709.2091.
[39] D. G. Figueroa, M. Hindmarsh, and J. Urrestilla, Phys. Rev. Lett. 110, **101302** (2013), 1212.5458.
[40] P. B. Arnold, G. D. Moore, and L. G. Yaffe, JHEP **0011**, 001 (2000), hep-ph/0010177.
[41] A. Megevand and F. A. Membiela (2013), 1311.2453.